



HAL
open science

Role of Ice Mechanics on Snow Viscoplasticity

Louis Védrine, Pascal Hagenmuller, Lionel Gélébart, Maurine Montagnat,
Antoine Bernard

► **To cite this version:**

Louis Védrine, Pascal Hagenmuller, Lionel Gélébart, Maurine Montagnat, Antoine Bernard.
Role of Ice Mechanics on Snow Viscoplasticity. *Geophysical Research Letters*, 2024, 51 (7),
pp.e2023GL107676. 10.1029/2023GL107676 . hal-04528866

HAL Id: hal-04528866

<https://hal.science/hal-04528866>

Submitted on 2 Apr 2024

HAL is a multi-disciplinary open access archive for the deposit and dissemination of scientific research documents, whether they are published or not. The documents may come from teaching and research institutions in France or abroad, or from public or private research centers.

L'archive ouverte pluridisciplinaire **HAL**, est destinée au dépôt et à la diffusion de documents scientifiques de niveau recherche, publiés ou non, émanant des établissements d'enseignement et de recherche français ou étrangers, des laboratoires publics ou privés.

Role of ice mechanics on snow viscoplasticity

Louis Védérine^{1,2}, Pascal Hagenmuller¹, Lionel Gélébart³, Maurine Montagnat^{1,4}, Antoine Bernard^{1,4}

¹Université Grenoble Alpes, Université de Toulouse, Météo-France, CNRS, CNRM, Centre d'Etudes de la Neige, Grenoble, France

²Université Paris-Saclay, ENS Paris-Saclay, DER Génie Civil et Environnement, Gif-sur-Yvette, France

³Université Paris-Saclay, CEA, Service de Recherches Métallurgiques Appliquées, 91191, Gif-sur-Yvette, France

⁴Univ. Grenoble Alpes, CNRS, IRD, G-INP, IGE, Grenoble, France

Key Points:

- Ice in snow cannot be considered as homogeneous, individual crystals are shown to impact snow creep.
- The models shows that basal glide of a few ice zones supports most of the snow deformation.
- In the simulations, the contribution of the hard slip systems is negligible, and deformation accommodation is enabled by the pore space.

Corresponding author: Pascal Hagenmuller, pascal.hagenmuller@meteo.fr

Abstract

The porous structure of snow becomes denser with time under gravity, primarily due to the creep of its ice matrix with viscoplasticity. Despite investigation of this behaviour at the macroscopic scale, the driving microscopic mechanisms are still not well understood. Thanks to high-performance computing and dedicated solvers, we modelled snow elasto-viscoplasticity with 3D images of its microstructure and different mechanical models of ice. The comparison of our numerical experiments to oedometric compression tests measured by tomography showed that ice in snow rather behaves as a heterogeneous set of ice crystals than as homogeneous polycrystalline ice. Similarly to dense ice, the basal slip system contributed at most, in the simulations, to the total snow deformation. However, in the model, the deformation accommodation between crystals was permitted by the pore space and did not require any prismatic and pyramidal slips, whereas the latter are pre-requisite for the simulation of dense ice.

Keywords: Viscoplasticity, Snow, Crystal, Microstructure, Tomography

Plain Language Summary

Knowledge of snow settlement is essential for many applications, such as paleoclimatology and avalanche forecasting. Snow densification is mainly driven by time dependent and irreversible deformations. Simulating this highly nonlinear behaviour for intricate microstructures is time-consuming, leading to a scarcity of studies and a limited understanding of the underlying microscale mechanisms. In this study, we took advantage of an advanced numerical solver to calculate the behaviour of 3D imaged snow samples and compared it with in situ experiments. Our analysis has shown that the crystalline structure must be taken into account, but the discrepancy between experiments and simulations suggests the existence of other mechanisms, particularly between snow grains. Interestingly, deformation mechanisms other than those required to simulate dense ice have been observed.

1 Introduction

Once on the ground, snow naturally settles under its weight. Its density typically increases from 100 kg m^{-3} just after its deposition on the ground to 550 kg m^{-3} at the end of the winter season at mid-latitude regions, up to the density of ice, 917 kg m^{-3} , for buried perennial snow on glaciers or ice sheets (Alley, 1987; Arnaud, Lipenkov, et al., 1998). The primary driving mechanisms of this settlement are the deformation of the ice skeleton of snow and the subsequent pore volume reduction (e.g., Yosida et al., 1958). Understanding the viscoplastic behaviour of snow is crucial to predict its densification, which is required to model the snowpack evolution (Lehning et al., 2002; Vionnet et al., 2012; Simson et al., 2021) or the pore close-off in ice cores (Gregory et al., 2014), which in turn relates to many applications such as avalanche forecasting (Morin et al., 2020), hydrology (DeBeer & Pomeroy, 2017) or paleo-climatology (Barnola et al., 1987).

The snow microstructure comprises open pores and sintered crystals of hexagonal ice (Ih). From a mechanical standpoint, the contribution of air is negligible, and snow mechanics thus depends solely on the spatial arrangement of these crystals and the deformation mechanisms they undergo. Under an overburden, isolated ice crystals essentially deform plastically by gliding of basal dislocations (Duval et al., 1983b). Non-basal dislocations were introduced in models to accommodate basal glide, but are poorly characterized (Hondoh, 2000). Their creep rate is at least two orders of magnitude lower than the one of the basal glide (Duval et al., 1983b). Ice crystals thus exhibit an extremely anisotropic viscoplastic behaviour. When the crystals are sintered together, the grain boundaries act as obstacles for dislocation movement, which results in hardening and more complex deformation mechanisms. For dense polycrystalline ice, these obstacles are max-

66 imal, and the high stresses generated at the crystal boundaries are thought to initiate
67 recrystallization: new crystals are nucleated and crystal boundaries migrate to replace
68 the highly distorted zones (Meyssonnier et al., 2009b; Montagnat et al., 2015). With in-
69 creasing porosity, the obstacles to dislocation at grain boundaries are successively reduced,
70 and grains can deform more independently from each other with the free space permit-
71 ted by the pores (Theile et al., 2011). For firn and snow with a density lower than 550 kg m^{-3} ,
72 an additional mechanism is thought to come into play: grain boundary sliding (Alley,
73 1987). It provides a convenient formalism for modeling firn densification (Lundin et al.,
74 2017; Schultz et al., 2022) but lacks experimental evidence so far (Meyssonnier et al., 2009b).

75 For snow with even lower density, less attention was drawn to the crystalline na-
76 ture of ice in snow (e.g., Shapiro et al., 1997). Only recently Riche et al. (2013); Calonne
77 et al. (2017); Montagnat et al. (2021) measured the crystallographic orientations statisti-
78 cally in snow. Indeed, the stress concentration in a few bearing force chains and bonds,
79 related to the shape and size of the ice skeleton (geometrical microstructure), is thought
80 to be the central control of the overall mechanical behaviour (Kry, 1975; Johnson & Hop-
81 kins, 2005; Wautier et al., 2017). However, the geometrical microstructure alone appears
82 insufficient to describe the diverse creep rates observed on different snow types (Calonne
83 et al., 2020; Fourteau et al., 2022). Besides, the driving deformation mechanism at the
84 microscale, either inter-crystalline deformation (e.g., grain boundary sliding) or (ii) intra-
85 crystalline deformation, remains a matter of debate because of a lack of experimental
86 evidence (Theile et al., 2011; Meyssonnier et al., 2009a; Sundu et al., 2024).

87 An alternative approach to understand and predict the mechanisms at play in snow
88 viscoplasticity relies on numerical experiments. The idea is to evaluate how different hy-
89 pothetical mechanisms in ice would affect the overall mechanical behaviour of snow. Ex-
90 perimental data, even if they do not exhibit the obvious signature of the involved mech-
91 anisms, can then be used to discriminate the modeling assumptions. The main ingre-
92 dients are the porous and crystalline microstructure of snow and the deformation mech-
93 anisms active in ice crystals and at their boundaries. Different studies followed this mod-
94 eling path in the last decades. Johnson and Hopkins (2005); Kabore et al. (2021) mod-
95 eled the snow microstructure as a set of solid discrete elements interacting with each other
96 through an elastic viscous-plastic contact law. By definition, this method describes the
97 dominant mechanism as grain boundary sliding. The snow viscosity simulated by Johnson
98 and Hopkins (2005); Peters et al. (2021) required an important scaling to reproduce ex-
99 perimental creep data of natural snow. However, the artificial microstructure used in the
100 simulation limits any 1:1 comparison to experimental data. In contrast, Theile et al. (2011);
101 Wautier et al. (2017) used a microstructure directly derived from tomographic data. They
102 only considered the deformation within the crystals and obtained a fair agreement with
103 experimental data. However, Theile et al. (2011) described the snow microstructure as
104 a collection of inter-connected finite element beams, which cannot reproduce deforma-
105 tion obstacles at the crystal boundaries. Wautier et al. (2017) described ice in snow as
106 a homogeneous material, polycrystalline ice. This approach is not suited to account for
107 the free space around ice crystals in snow, which may favour basal dislocations glide, in
108 contrast to dense polycrystalline ice.

109 In line with these previous studies, we aim to quantify the effect of ice mechanics
110 on snow viscoplasticity. We use time-series of three-dimensional images obtained via to-
111 mography during mechanical tests as direct inputs of a mechanical model. The mate-
112 rial law for ice in the snow is either homogeneous polycrystalline ice (*ice foam model*),
113 or each crystal is associated with a given crystal plasticity model (*sintered crystal model*).
114 This general approach avoids any over-simplification of the snow microstructure and the
115 ice mechanics.

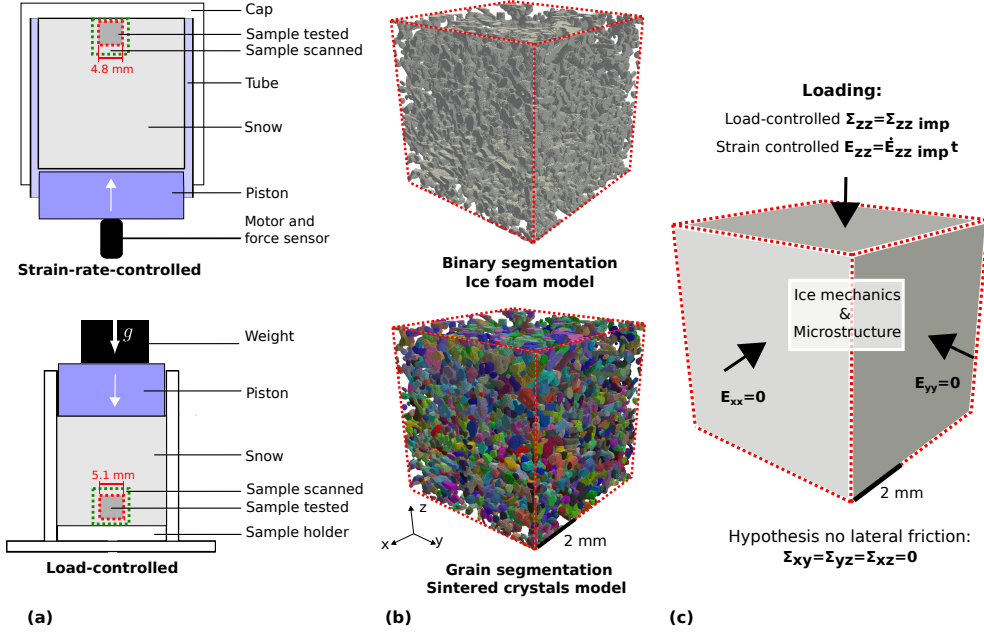


Figure 1. Main workflow. (a) Schemes of the mechanical tests. (b) 3D snow microstructure image used for the simulation: binary ice-air image for the ice foam model (top), grain image for the sintered crystal model (bottom). (c) Numerical set-up and boundary conditions.

2 Material and Methods

2.1 Experimental data

We used two different mechanical tests: a strain-rate-controlled experiment (Bernard, 2023) and a load-controlled experiment (Bernard et al., 2022) (Fig.1a). In these tests, the macroscopic stress or strain was measured, and the microstructure was regularly scanned at a micro-metric resolution in an X-ray tomograph (DeskTom130, RXSolutions). The experiments were conducted under isothermal conditions on natural snow that was let evolve in a cold room at respectively -20 °C and -6 °C for several weeks. Experimental conditions and imaging setup are summarized in Table 1, and detailed in Bernard et al. (2022); Bernard (2023).

The greyscale attenuation images measured by tomography were binary segmented into pore space and a continuous ice matrix (Hagenmuller et al., 2013; Bernard et al., 2022) (Fig.1b top). This data does not contain any information about crystal boundaries. The ice matrix was thus segmented into individual grains based on two geometrical criteria: negative minimal principal curvature and low contiguity between the grains (Hagenmuller, Chambon, et al., 2014; Peinke et al., 2020) (Fig.1b bottom). We assumed that the grains detected by the algorithm correspond to the ice crystals, which is reasonable for this type of snow according to Arnaud, Gay, et al. (1998).

2.2 Numerical model

2.2.1 Constitutive law for ice

A key ingredient of the numerical model is the elasto-viscoplastic law used for ice. The strain tensor in ice can be decomposed as the sum of an elastic and a viscoplastic part: $\epsilon = \epsilon^e + \epsilon^{vp}$. The elastic strain ϵ^e is related to the stress tensor σ and the stiffness tensor \mathbf{C} as $\sigma = \mathbf{C} : \epsilon^e$. The viscoplastic strain rate $\dot{\epsilon}^{vp}$ is related to the stress

Table 1. Experimental conditions of the mechanical tests. The type of snow is defined according to (Fierz et al., 2009), where DF stands for Decomposing and Fragmented snow, and RG stands for Rounded Grains. The numbers shown in brackets, e.g., $[a, b]$, mean that the parameter ranges between, e.g., a and b . Details can be found in the associated references.

Parameter	Load-controlled	Strain-rate-controlled
Temperature (°C)	-8 ± 0.5	-18.5 ± 0.5
Type of snow	DF	DF/RG
Initial density (kg m^{-3})	230	206
Initial specific surface area ($\text{m}^2 \text{kg}^{-1}$)	30	28
Test duration (days)	5	3.5
Strain rate (s^{-1})	$[10^{-8}, 10^{-7}]$	1.8×10^{-6}
Stress (kPa)	2.1	$[0, 300]$
Sample size: diameter (mm) x height (mm)	35×38	14×14
Image cubic side-length (voxel)	900	800
Image resolution (μm)	8.5	8
X-ray voltage (kV)	50	50
X-ray current (μA)	160	160
Number of scans	14	11
Typical strain between scans (%)	0.5	5
Reference	Bernard et al. (2022)	Bernard (2023)

140 tensor $\boldsymbol{\sigma}$ as $\dot{\boldsymbol{\epsilon}}^{vp} = f(\boldsymbol{\sigma})$. The values of \mathbf{C} or f depend on whether ice is considered a
 141 homogeneous material or a set of sintered single-crystals.

142 *Ice foam model.* Ice in snow can be considered homogeneous polycrystalline ice, where
 143 the contributions of each crystal are averaged as in dense ice (Mellor, 1975; Theile et al.,
 144 2011; Wautier et al., 2017). The elasticity tensor of the ice matrix \mathbf{C} is then isotropic
 145 and described by the Young’s modulus $E = 9$ GPa and the Poisson ratio $\nu = 0.3$ (Petrovic,
 146 2003). The viscous part of pure dense ice is described by a 3D Norton-Hoff law as (Gagliardini
 147 & Meyssonier, 1999):

$$\dot{\boldsymbol{\epsilon}}^{vp} = \frac{3}{2} A \sigma_{eq}^{n-1} \boldsymbol{\sigma}' \quad (1)$$

148 where $\boldsymbol{\sigma}'$ is the deviatoric stress tensor and $\sigma_{eq} = \sqrt{\frac{3}{2} \boldsymbol{\sigma}' : \boldsymbol{\sigma}'}$ is the Von Mises equiv-
 149 alent stress and $A = 7.8 \times 10^{-8} \text{ MPa}^{-n} \text{ s}^{-1}$ at -10°C and $n = 3$ (Budd & Jacka, 1989;
 150 Castelnau et al., 1997; Theile et al., 2011).

151 *Sintered crystal model.* Ice in snow can also be explicitly modelled as a set of in-
 152 dividual ice crystals sintered together, each characterized by a large viscoplastic anisotropy.
 153 Since the crystalline orientation is not captured by tomography, it was randomly sam-
 154 pled in an isotropic distribution (see Text S3 and Fig. S4 for sensitivity analysis). The
 155 elasticity tensor \mathbf{C} was supposed to be isotropic transverse in the crystal reference frame
 156 and defined according to Gammon et al. (1983) ($C_{11} = 13.9$ GPa, $C_{33} = 15.0$ GPa,
 157 $C_{44} = 3.0$ GPa, $C_{12} = 7.1$ GPa, $C_{13} = 5.8$ GPa). For the viscoplastic part, we used
 158 the crystal plasticity model of Lebensohn et al. (2009). In this model, ice crystals can
 159 deform through slip on three soft basal systems, three hard prismatic systems, and six
 160 hard pyramidal systems (Montagnat et al., 2014). On the k -th system, the slip-rate $\dot{\gamma}^{(k)}$

161 is related to the shear stress $\tau^{(k)}$ by

$$\dot{\gamma}^{(k)} = \dot{\gamma}_0^{(k)} \left(\frac{|\tau^{(k)}|}{\tau_0^{(k)}} \right)^{n^{(k)}} \text{sign}(\tau^{(k)}) \quad (2)$$

162 with $n^{(k)}$ the stress exponent, $\dot{\gamma}_0^{(k)}$ the reference shear-rate and $\tau_0^{(k)}$ the critical shear stress.
 163 The critical stresses $\tau_0^{(k)}$ for the prismatic and pyramidal systems were assumed to be
 164 constant (no hardening) and equal to 260 MPa, which is 20 times larger than the val-
 165 ues chosen for the basal systems (13 MPa). For all systems, the creep exponent is $n^{(k)} =$
 166 3 and the reference shear-rate is $\dot{\gamma}_0^{(k)} = 1 \text{ s}^{-1}$. This setup enables to reproduce the be-
 167 haviour of polycrystalline ice, when the single crystals are randomly arranged into a dense
 168 packing (Text. S1 in Supporting Information). This model, although simpler than Suquet
 169 et al. (2012), was preferred for the sintered crystal model, as it allows a simple compar-
 170 ison with the foam model, giving the same stress exponent n on the macroscopic scale.

171 To account for temperature effects on ice viscoplasticity, we scaled the pre-factor
 172 A of the ice foam model (Eq. 1) and the pre-factor $\dot{\gamma}_0^{(k)}$ of the crystal model (Eq. 2) by
 173 an Arrhenius relation: $e^{-\frac{Q}{RT}}$, with $Q = 69.1 \text{ kJ mol}^{-1}$ the activation energy of ice, $R =$
 174 $8.3 \text{ J (mol K)}^{-1}$ the universal gas constant and T the temperature (K) (Mellor & Testa,
 175 1969). This scaling enables us to account for the different temperatures in the two ex-
 176 periments ($-8 \text{ }^\circ\text{C}$ and $-18.5 \text{ }^\circ\text{C}$, Tab. 1).

177 2.2.2 Simulation set-up

178 The simulations were performed with the Fast Fourier Transform (FFT)-based solver
 179 AMITEX_FFTP (Gélébart et al., 2020). This solver takes as direct input the 3D air-ice
 180 image (ice foam model) or the 3D image of the crystal assembly (sintered crystal model).
 181 The numerical model cannot account for topological change of the ice skeleton (e.g., new
 182 contacts). The simulation of one experiment thus consists of several simulations of “in-
 183 stantaneous creep experiments” as in Theile et al. (2011), with initial conditions vary-
 184 ing through the test (re-set at each new image). The Norton-Hoff model and the crystal
 185 plasticity model were implemented through the MFront code generator (Helfer et al.,
 186 2015). The numerical integration of crystal plasticity is computationally expensive, but
 187 the solver benefits from the MPI implementation.

188 Using an FFT-based solver involves using periodic boundary conditions. The bound-
 189 ary conditions were chosen to mimic the mechanical tests, where the snow sample can-
 190 not deform laterally and the axial friction on the sample holder is limited. Therefore,
 191 in the simulation, we imposed the average lateral deformation ($E_{xx} = E_{yy} = 0$) and
 192 the shear stress to zero ($\Sigma_{xy} = \Sigma_{yz} = \Sigma_{xz} = 0$), where E and Σ are respectively the
 193 volume average of strain and stress. The axial loading was imposed according to the type
 194 of test (Fig.1c).

195 To reduce the computation time, the simulations were not conducted on the en-
 196 tire scanned volume at the nominal image resolution. Instead, we reduced the resolu-
 197 tion by a factor of 2, i.e. to voxels of size 16 and 17 microns respectively for the strain-
 198 rate-controlled and load-controlled experiments, and we extracted a volume of $300 \times 300 \times$
 199 300 voxels inside the scans (Fig. 1). We performed a volume convergence analysis on one
 200 sample and showed that the chosen volume and resolution are representative of the sam-
 201 ple. To fasten the solver convergence, we reduced the infinite mechanical contrast be-
 202 tween ice and air to $E_{\text{ice}}/E_{\text{air}} = 10^8$ by giving a very small stiffness to air. We observed
 203 that this choice reduced the computing cost and did not affect the results (Fig. S2).

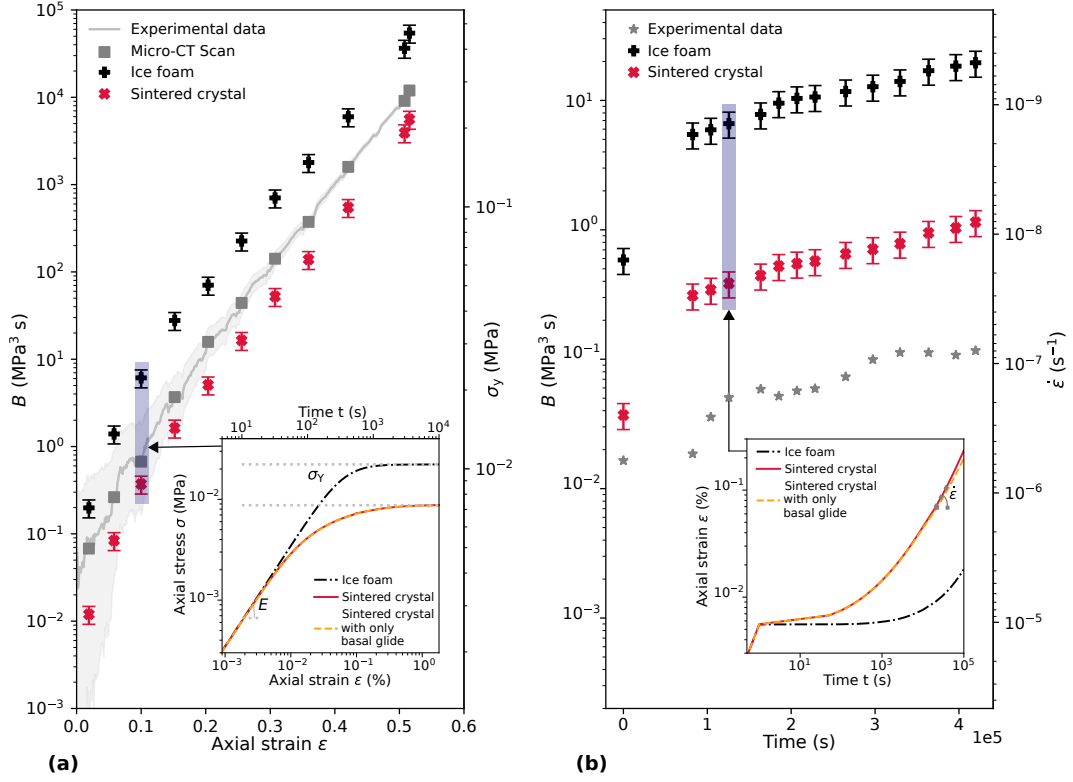


Figure 2. Comparison of the experimental and numerical results. **(a)** Evolution of the non-linear viscosity and the yield stress as a function of strain (strain-rate-controlled). **(b)** Temporal evolution of the nonlinear viscosity and the strain rate (load-controlled). The inset figures correspond to the simulated macroscopic stress or strain evolution for different constitutive materials for a given microstructure. The error bars are related to the limited simulation volume (error of $\pm 14.9\%$, Fig. S3), the resolution decrease (error $\pm 16.4\%$, Fig. S3) and uncertainties on temperature (error of $\pm 6.2\%$ at $-8\text{ }^\circ\text{C}$ and $\pm 6.8\%$ at $-18.5\text{ }^\circ\text{C}$).

204 3 Results and discussion

205 3.1 Simulated macroscopic stress-strain curve

206 We observe three different regimes of stress evolution with strain during the com-
 207 pression test at a constant strain-rate (Fig.2a inset). First, the stress increases linearly
 208 with strain in an elastic regime characterized by a slope E . Then, the stress deviates from
 209 elasticity with viscoplasticity progressively activated. After this transient regime, the stress
 210 eventually reaches a constant value, the yield stress σ_Y , where the snow sample perfectly
 211 flows (stationary creep). This yield stress depends on the constitutive law of ice and the
 212 snow microstructure. Similarly, Figure 2b (inset) shows the time evolution of strain under
 213 constant stress. After a brief phase of pure elasticity during the numerical loading
 214 of the sample (stress from 0 to 2.1 kPa in 1 s), the ice matrix starts to flow and the strain
 215 rate increases to a constant value.

216 The permanent viscoplastic regime is reached after a typical strain of 0.1% (Fig.
 217 2a) or a time of 10^4 s (Fig. 2b). The yield stress or flow rate are, hereafter, derived at
 218 a simulation strain of 0.5% and a simulation time of 10^5 s. The time or strain required
 219 to reach the stationary creep flow regime is relatively small compared to the time be-
 220 tween two scans (~ 8 h) or change in the microstructure. Therefore, the assumption that
 221 mechanical creep experiments with an evolving microstructure can be decomposed into
 222 “instantaneous creep experiments” seems reasonable. In other words, this separation of
 223 time scales enables us to compare the yield stress estimated numerically on a given mi-
 224 crostructure to the stress measured when the microstructure was captured (Theile et al.,
 225 2011).

226 The elastic and viscoplastic regimes were simulated with different models for ice.
 227 The stiffness of the sample is not affected by the modelling assumptions, i.e. the slight
 228 anisotropy of crystalline elasticity (30%) could be neglected. Indeed, a relative error of
 229 0.5% is committed on the axial Young’s modulus with the ice foam model compared to
 230 the sintered crystal model. Therefore, assuming ice in snow as a foam of ice to study snow
 231 elasticity (Schneebeli, 2004; Srivastava et al., 2010; Köchle & Schneebeli, 2014; Hagen-
 232 muller, Theile, & Schneebeli, 2014; Hagenmuller, Calonne, et al., 2014; Wautier et al.,
 233 2015; Reuter et al., 2019) appears reasonable, even never properly evaluated so far. In
 234 contrast, the simulated viscoplastic regime is very different between the ice foam and the
 235 sintered crystal models. For instance, at a strain rate of $1.8 \times 10^{-6} \text{ s}^{-1}$, a yield stress
 236 of 22.2 kPa and 8.7 kPa is obtained respectively for the ice foam and sintered crystal mod-
 237 els (Fig. 2a). As expected, the crystal model makes the snow sample flow more easily.
 238 Interestingly, blocking the hard slip systems of the sintered crystal model (only basal glide)
 239 does not significantly affect the macroscopic mechanical behaviour of the snow for both
 240 experiments.

241 As the snow stress strain-rate relation is non-linear, the classical compactive vis-
 242 cosity cannot describe both tests (Kojima, 1967). The creep exponent of all slip systems
 243 is here constant ($n = 3$). Therefore, per homogenization, this exponent scales to the
 244 visco-plastic model of snow (Wautier et al., 2017) and we can identify the observed creep
 245 of snow by a Glen’s law with a non-linear viscosity B :

$$\dot{\epsilon}_{snow} = \frac{1}{B} \sigma_Y^n \quad (3)$$

246 3.2 Evaluation of the numerical model with the experiments

247 In the strain-rate-controlled experiment, the measured non-linear viscosity B in-
 248 creases from 6.8×10^{-2} to $1.2 \times 10^4 \text{ MPa}^{-n} \text{ s}^{-1}$, while the density increases from 206
 249 to 458 kg m^{-3} (Fig. 2). The simulations well reproduce this trend with density, and the
 250 order of magnitude of B . For a similar density range, Scapozza and Bartelt (2003) ob-
 251 tained a viscosity change from 10^{-2} to $10^6 \text{ MPa}^{-n} \text{ s}^{-1}$ at a temperature of -12°C . Note

252 that in this experiment, the exponent of Glen’s law was identified experimentally, and
 253 varies from 1.7 for a density of 150 kg m⁻³ to 3.7 for a density of 423 kg m⁻³. In the
 254 load-controlled experiment, the increase of the non-linear viscosity with time is less pro-
 255 nounced, as the overall deformation or densification remains rather small ($\epsilon_z \leq 9.1\%$).
 256 However, the simulation also reproduces this tedious trend driven by microstructure evo-
 257 lution.

258 The simulations with the sintered crystal and the ice foam model respectively un-
 259 derestimate and overestimate B in the strain-rate-controlled experiment. The measured
 260 and simulated value of B at the beginning of the experiment is uncertain due to the lim-
 261 ited resolution of the force sensor (± 4 kPa). However, for stresses higher than 25 kPa,
 262 we observe that the sintered crystals model is closer to the experimental measurements,
 263 than the foam model. Indeed, the mean absolute percentage error (MAPE) between sim-
 264 ulations and the experiments is equal to 414% for the ice foam model and to 62% for the
 265 sintered crystal model. The difference between the sintered crystal and the ice foam mod-
 266 els reduces when density increases. The ratio decreases from 16.6 at a density of 206 kg m⁻³,
 267 to 9.7 at a density of 458 kg m⁻³. This is consistent with the fact that the two models
 268 converge together when the porous structure becomes pure ice (see Supp. Inf. S1 and
 269 A. Lebensohn (2001)). More generally, we expect that the models become closer when
 270 the crystal boundaries become pre-dominant barriers to basal dislocation glide.

271 For the load-controlled experiment, the simulations based on the sintered crystal
 272 model are closer to the experiment (over-estimation of B by an average factor of 8.9) com-
 273 pared to the ones based on the ice foam model (over-estimation of B by 157). Note that
 274 the error factor estimated here on the non-linear viscosity are raised to the power of 3
 275 compared to the errors computed on linear viscosity ($\eta = \frac{\sigma}{\dot{\epsilon}}$), as it is presented by (Kojima,
 276 1967; Theile et al., 2011). Experimental uncertainties also exist in the load-controlled
 277 test (Figure 2b), but they are difficult to estimate and related to i) the measurement of
 278 the strain rate and ii) the force effectively applied to the considered snow volume. Nev-
 279 ertheless, they can be estimated to be less than the ratio 8.9 between the best model and
 280 the experiment.

281 Overall, for snow, here with a density in the range 206 to 458 kg m⁻³, the two mod-
 282 els for ice yield very different viscoplastic properties, and the sintered crystal model ap-
 283 pears to be closer to the experimental data. This observation agrees with the recent work
 284 of Fourteau et al. (2023), who shows that it is impossible to find a calibrated isotropic
 285 law to represent different types of microstructures, and questions the magnitude of non-
 286 linear viscosity simulated by Wautier et al. (2017). Nevertheless, the significant discrep-
 287 ancies between the sintered crystal model and experiments show that some mechanisms
 288 may still be missing in this modelling.

289 3.3 Microscale drivers of snow viscoplasticity

290 In the sintered crystal model, we observe that a small deformation of the ice ma-
 291 trix yields important deformation of the pore space and the overall snow material. In-
 292 deed, the average deformation of the ice matrix is here typically 100 times smaller than
 293 in the equivalent snow material (Fig. S4). In addition, the distribution of strain or stresses
 294 in the ice matrix itself is highly heterogeneous (standard deviation of 30% on strain in
 295 the ice matrix) and comprises both zones in tension and compression (noted with a pos-
 296 itive sign) (Fig. 3). For instance, 4% of the ice volume exhibits an axial deformation 10
 297 times larger than the average ice deformation, while a significant part (e.g., 34.5%) of
 298 the microstructure exhibits almost no deformation (e.g., $|\epsilon_z| \leq 0.1\bar{\epsilon}_z$). This confirms
 299 previous numerical observations on elastic properties (Hagenmuller, Theile, & Schnee-
 300 beli, 2014) but is here even more pronounced as the ice can locally undergo large vis-
 301 coplastic deformation.

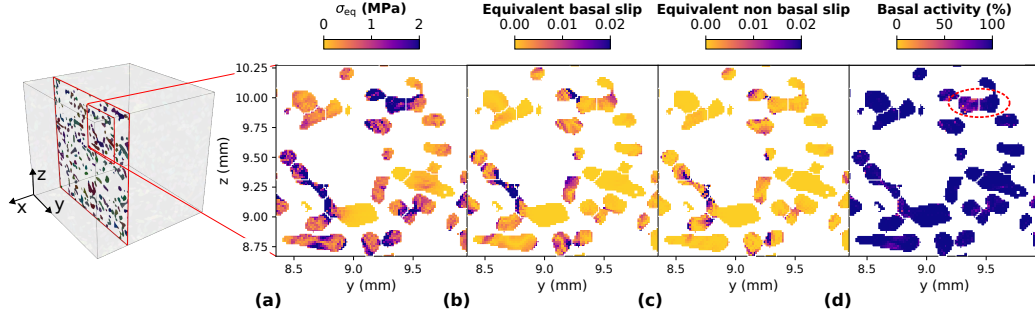


Figure 3. Slice view of the tested sample shown in figure 1 and associated mechanical fields: (a) Von Mises equivalent stress σ_{eq} . (b) Equivalent viscoplastic basal slip. (c) Equivalent viscoplastic non basal slip. (d) Basal activity. Strain-rate-controlled experiment, axial stress corresponding to this microstructure of 8.7 kPa.

302 Interestingly, similarly to dense ice, the basal slip system contributes at most to
 303 the total simulated plastic deformation of snow (90% in average for ice, 99% for snow,
 304 see Fig. S4). However, the entanglement of slip system deformations appears to be dif-
 305 ferent between snow and dense ice. The model shows that the deformation accommo-
 306 dation between crystals is permitted by the pore space and does not require prismatic
 307 and pyramidal slips, whereas the latter are pre-requisite for the simulation of any de-
 308 formation in dense ice. In addition, blocking the hard slip systems of the sintered crys-
 309 tal model does not significantly affect the macroscopic mechanical behaviour of the snow
 310 for both experiments (Fig. 2). Thus, a stronger effect of the basal system parameteri-
 311 zation on the macroscopic response of the snow can be expected. Indeed, the chosen pa-
 312 rameterization was mostly evaluated on pure ice experiments (Castelnaud et al., 1996, 1997;
 313 Mansuy et al., 2000), but different choice for the basal slip system (e.g., exponent n or
 314 critical shear stress τ_0) might yield similar results for polycrystalline ice but not for snow
 315 (Duval et al., 1983a; Suquet et al., 2012).

316 Stresses and strains are heterogeneously distributed in the microstructure and gen-
 317 erally located at necks between ice grains that participate in a force bearing chain (Fig.
 318 3). These geometric necks also mainly correspond, here, to the crystal boundaries. The
 319 grain boundaries (defined as a one voxel wide band on either side of the interface between
 320 2 grains, which represent 11% of the ice volume fraction), concentrate 20.5% of the equiv-
 321 alent stress, 21% of basal equivalent strain and 22.2% of non-basal equivalent strain. When
 322 we do not account anymore for the single crystals (i.e., foam model), the stress concen-
 323 tration reduces to 17% of the equivalent stress. This stress concentration is thus not only
 324 linked to the geometry of the microstructure, but also to the mechanical model of ice.
 325 Interestingly, the relative basal activity remains high everywhere. It is lower next to cer-
 326 tain crystal boundaries, where the stresses are the highest (Fig. 3d). Non-basal contri-
 327 butions also appear in crystals with very little plastic deformation but large stress concen-
 328 tration (e.g., the grain circled in Fig. 3). This observation indicates that crystal bound-
 329 aries may slightly limit basal slip, but in a proportion that is not visible on the overall
 330 viscous behaviour (here for a snow sample with a density of 235 kg m^{-3}).

331 4 Conclusion

332 We simulated the viscoplasticity of snow based on its 3D microstructure and dif-
 333 ferent constitutive laws for the ice matrix. These numerical experiments were compared
 334 to cold-room in-tomograph experiments, either load-controlled or strain-rate-controlled.
 335 The macro-scale comparison revealed that ice in snow rather behaves as a set of sintered

336 crystals than a foam of polycrystalline ice. Moreover, we showed that the accommoda-
 337 tion of deformation by means of the hard non-basal slip systems is hardly needed, even
 338 less than for bulk polycrystalline ice. This is attributed to the ability to relax strain in-
 339 compatibilities at ice / air interfaces. The residual mismatch between the measured and
 340 the simulated viscosity tends to demonstrate that other mechanisms occurring, e.g., at
 341 bonds need to be accounted for, such as, role of non-basal contributions with harden-
 342 ing (Duval et al., 1983a; Suquet et al., 2012), superplasticity (Alley, 1987; Raj & Ashby,
 343 1971; Goldsby & Kohlstedt, 2001; Sundu et al., 2024), but also ductile failure (Kirchner
 344 et al., 2001; Capelli et al., 2020).

345 Open Research

346 All materials used in this article (codes, segmented images, experimental and nu-
 347 merical values, etc.) are available on Zenodo at <https://doi.org/10.5281/zenodo.10340967>
 348 (Védrine et al., 2023).

349 Acknowledgments

350 TomoCold was funded by the CNRM and INSU-LEFE, Labex OSUG (ANR10 LABX56).
 351 This work has been supported by program (ANR15 IDEX02). The computations pre-
 352 sented in this paper were performed using the GRICAD infrastructure ([https://gricad
 353 .univ-grenoble-alpes.fr](https://gricad.univ-grenoble-alpes.fr)), which is supported by CNRS, University Grenoble Alpes
 354 and INRIA. We particularly thank Mr. Mondher CHEKKI for his help.

355 References

- 356 A. Lebensohn, R. (2001). N-site modeling of a 3d viscoplastic polycrystal using fast
 357 fourier transform. *Acta Materialia*, *49*(14), 2723-2737. doi: [https://doi.org/
 358 https://doi.org/10.1016/S1359-6454\(01\)00172-0](https://doi.org/https://doi.org/10.1016/S1359-6454(01)00172-0)
- 359 Alley, R. B. (1987, 3). Firn densification by grain-boundary sliding: a first model.
 360 *Le Journal de Physique Colloques*, *48*(C1), 1-249. Retrieved from [http://www
 361 .edpsciences.org/10.1051/jphyscol:1987135](http://www.edpsciences.org/10.1051/jphyscol:1987135) doi: [https://doi.org/10
 362 .1051/jphyscol:1987135](https://doi.org/10.1051/jphyscol:1987135)
- 363 Arnaud, L., Gay, M., Barnola, J.-M., & Duval, P. (1998, 1). Imaging of firn and
 364 bubbly ice in coaxial reflected light: a new technique for the characteriza-
 365 tion of these porous media. *Journal of Glaciology*, *44*(147), 326-332. doi:
 366 <https://doi.org/10.3189/S0022143000002653>
- 367 Arnaud, L., Lipenkov, V., Barnola, J.-M., Gay, M., & Duval, P. (1998). Modelling of
 368 the densification of polar firn: characterization of the snow-firn transition. *An-
 369 nals of Glaciology*, *26*, 39-44.
- 370 Barnola, J.-M., Raynaud, D., Korotkevich, Y. S., & Lorius, C. (1987). Vostok ice
 371 core provides 160,000-year record of atmospheric CO₂. *Nature*, *329*(6138),
 372 408-414. Retrieved from <https://doi.org/10.1038/329408a0> doi:
 373 <https://doi.org/10.1038/329408a0>
- 374 Bernard, A. (2023). *Etude multiéchelle de la transition ductile-fragile dans la neige*
 375 (Doctoral dissertation, Université Grenoble Alpes). Retrieved from [https://
 376 theses.hal.science/tel-04145610](https://theses.hal.science/tel-04145610)
- 377 Bernard, A., Hagenmuller, P., Montagnat, M., & Chambon, G. (2022, 12). Dis-
 378 entangling creep and isothermal metamorphism during snow settlement with
 379 X-ray tomography. *Journal of Glaciology*, 1-12. Retrieved from [https://
 380 www.cambridge.org/core/product/identifier/S0022143022001095/type/
 381 journal_article](https://www.cambridge.org/core/product/identifier/S0022143022001095/type/journal_article) doi: <https://doi.org/10.1017/jog.2022.109>
- 382 Budd, W., & Jacka, T. (1989, 7). A review of ice rheology for ice sheet mod-
 383 elling. *Cold Regions Science and Technology*, *16*(2), 107-144. Retrieved from
 384 <https://linkinghub.elsevier.com/retrieve/pii/0165232X89900141> doi:

- 385 [https://doi.org/10.1016/0165-232X\(89\)90014-1](https://doi.org/10.1016/0165-232X(89)90014-1)
- 386 Calonne, N., Montagnat, M., Matzl, M., & Schneebeli, M. (2017). The layered
387 evolution of fabric and microstructure of snow at point barnola, central
388 east antarctica. *Earth and Planetary Science Letters*, *460*, 293-301. doi:
389 <https://doi.org/https://doi.org/10.1016/j.epsl.2016.11.041>
- 390 Calonne, N., Richter, B., Löwe, H., Cetti, C., Ter Schure, J., van Herwijnen, A.,
391 ... Schneebeli, M. (2020). The RHOSSA campaign: Multi-resolution
392 monitoring of the seasonal evolution of the structure and mechanical sta-
393 bility of an alpine snowpack. *The Cryosphere*, *14*(6), 1829–1848. doi:
394 <https://doi.org/10.5194/tc-14-1829-2020>
- 395 Capelli, A., Reiweger, I., & Schweizer, J. (2020, 7). Studying Snow Failure With
396 Fiber Bundle Models. *Frontiers in Physics*, *8*(July), 1–12. Retrieved from
397 <https://www.frontiersin.org/article/10.3389/fphy.2020.00236/full>
398 doi: <https://doi.org/10.3389/fphy.2020.00236>
- 399 Castelnau, O., Canova, G. R., Lebensohn, R. A., & Duval, P. (1997). Modelling
400 viscoplastic behavior of anisotropic polycrystalline ice with a self-consistent ap-
401 proach. *Acta Materialia*, *45*(11), 4823–4834. doi: [https://doi.org/10.1016/S1359-6454\(97\)00098-0](https://doi.org/10.1016/S1359-6454(97)00098-0)
- 402
- 403 Castelnau, O., Duval, P., Lebensohn, R. A., & Canova, G. R. (1996). Viscoplastic
404 modeling of texture development in polycrystalline ice with a self-consistent
405 approach: Comparison with bound estimates. *Journal of Geophysical Research: Solid Earth*, *101*(B6), 13851–13868.
- 406
- 407 DeBeer, C. M., & Pomeroy, J. W. (2017, 10). Influence of snowpack and melt
408 energy heterogeneity on snow cover depletion and snowmelt runoff simu-
409 lation in a cold mountain environment. *Journal of Hydrology*, *553*, 199–
410 213. Retrieved from <https://linkinghub.elsevier.com/retrieve/pii/S0022169417305164>
411 doi: <https://doi.org/10.1016/j.jhydrol.2017.07.051>
- 412
- 413 Duval, P., Ashby, M., & Anderman, I. (1983a). Rate-controlling processes in the
414 creep of polycrystalline ice. *The Journal of Physical Chemistry*, *87*(21), 4066–
415 4074.
- 416 Duval, P., Ashby, M. F., & Anderman, I. (1983b, 10). Rate-controlling processes
417 in the creep of polycrystalline ice. *The Journal of Physical Chemistry*,
418 *87*(21), 4066–4074. Retrieved from <https://pubs.acs.org/doi/10.1021/j100244a014>
419 doi: <https://doi.org/10.1021/j100244a014>
- 420 Fierz, C., Durand, R., Etchevers, Y., Greene, P., McClung, D. M., Nishimura, K., ...
421 Sokratov, S. A. (2009). *The international classification for seasonal snow on*
422 *the ground* (Tech. Rep.). Paris: IHP-VII Technical Documents in Hydrology
423 N83, IACS Contribution N1, UNESCO-IHP.
- 424 Fourteau, K., Freitag, J., Malinen, M., & Löwe, H. (2023). Microstructure-based
425 simulations of the viscous densification of snow and firn. *EGUsphere*, *2023*, 1–
426 26.
- 427 Fourteau, K., Löwe, H., & Freitag, J. (2022). Microstructure-based simulations of
428 the compactive viscosity of snow and firn with isotropic and anisotropic ma-
429 terial laws. In *International symposium on snow*. Davos, Switzerland, 25-30
430 September 2022.
- 431 Gagliardini, O., & Meyssonier, J. (1999). Analytical derivations for the behav-
432 ior and fabric evolution of a linear orthotropic ice polycrystal. *Journal of Geo-*
433 *physical Research: Solid Earth*, *104*(B8), 17797-17809. doi: <https://doi.org/https://doi.org/10.1029/1999JB900146>
- 434
- 435 Gammon, P. H., Kieft, H., Clouter, M. J., & Denner, W. W. (1983). Elastic
436 constants of artificial and natural ice samples by Brillouin spectroscopy.
437 *Journal of Glaciology*, *29*(103), 433–460. doi: <https://doi.org/10.1017/S0022143000030355>
- 438
- 439 Gélébart, L., Derouillat, J., Doucet, N., Ouaki, F., Marano, A., & Duverge, J.

- 440 (2020). *AMITEX_FFTP*.
- 441 Goldsby, D., & Kohlstedt, D. L. (2001). Superplastic deformation of ice: Exper-
442 imental observations. *Journal of Geophysical Research: Solid Earth*, 106(B6),
443 11017–11030.
- 444 Gregory, S. A., Albert, M. R., & Baker, I. (2014). Impact of physical properties and
445 accumulation rate on pore close-off in layered firn. *Cryosphere*, 8(1), 91–105.
446 doi: <https://doi.org/10.5194/tc-8-91-2014>
- 447 Hagenmuller, P., Calonne, N., Chambon, G., Flin, F., Geindreau, C., & Naaim,
448 M. (2014, 12). Characterization of the snow microstructural bonding sys-
449 tem through the minimum cut density. *Cold Regions Science and Tech-*
450 *nology*, 108, 72–79. Retrieved from [https://linkinghub.elsevier.com/](https://linkinghub.elsevier.com/retrieve/pii/S0165232X1400161X)
451 [retrieve/pii/S0165232X1400161X](https://linkinghub.elsevier.com/retrieve/pii/S0165232X1400161X) doi: [https://doi.org/10.1016/](https://doi.org/10.1016/j.coldregions.2014.09.002)
452 [j.coldregions.2014.09.002](https://doi.org/10.1016/j.coldregions.2014.09.002)
- 453 Hagenmuller, P., Chambon, G., Flin, F., Morin, S., & Naaim, M. (2014, 8).
454 Snow as a granular material: assessment of a new grain segmentation al-
455 gorithm. *Granular Matter*, 16(4), 421–432. Retrieved from [http://](http://link.springer.com/10.1007/s10035-014-0503-7)
456 link.springer.com/10.1007/s10035-014-0503-7 doi: [https://doi.org/](https://doi.org/10.1007/s10035-014-0503-7)
457 [10.1007/s10035-014-0503-7](https://doi.org/10.1007/s10035-014-0503-7)
- 458 Hagenmuller, P., Chambon, G., Lesaffre, B., Flin, F., & Naaim, M. (2013,
459 7). Energy-based binary segmentation of snow microtomographic im-
460 ages. *Journal of Glaciology*, 59(217), 859–873. Retrieved from [https://](https://www.cambridge.org/core/product/identifier/S0022143000202852/type/journal_article)
461 [www.cambridge.org/core/product/identifier/S0022143000202852/type/](https://www.cambridge.org/core/product/identifier/S0022143000202852/type/journal_article)
462 [journal_article](https://www.cambridge.org/core/product/identifier/S0022143000202852/type/journal_article) doi: <https://doi.org/10.3189/2013JoG13J035>
- 463 Hagenmuller, P., Theile, T. C., & Schneebeli, M. (2014, 1). Numerical simulation
464 of microstructural damage and tensile strength of snow. *Geophysical Research*
465 *Letters*, 41(1), 86–89. Retrieved from [http://doi.wiley.com/10.1002/](http://doi.wiley.com/10.1002/2013GL058078)
466 [2013GL058078](http://doi.wiley.com/10.1002/2013GL058078) doi: <https://doi.org/10.1002/2013GL058078>
- 467 Helfer, T., Michel, B., Proix, J. M., Salvo, M., Sercombe, J., & Casella, M. (2015).
468 Introducing the open-source mfront code generator: Application to mechanical
469 behaviours and material knowledge management within the PLEIADES fuel
470 element modelling platform. *Computers and Mathematics with Applications*,
471 70(5), 994–1023. Retrieved from [http://dx.doi.org/10.1016/j.camwa.2015](http://dx.doi.org/10.1016/j.camwa.2015.06.027)
472 [.06.027](http://dx.doi.org/10.1016/j.camwa.2015.06.027) doi: <https://doi.org/10.1016/j.camwa.2015.06.027>
- 473 Hondoh, T. (2000). Nature and behavior of dislocations in ice. In T. Hondoh (Ed.),
474 *Physics of ice core records* (p. 2-34). Sapporo: Hokkaido University Press.
- 475 Johnson, J. B., & Hopkins, M. A. (2005, 9). Identifying microstructural deformation
476 mechanisms in snow using discrete-element modeling. *Journal of Glaciol-*
477 *ogy*, 51(174), 432–442. Retrieved from [https://www.cambridge.org/core/](https://www.cambridge.org/core/product/identifier/S0022143000209507/type/journal_article)
478 [product/identifier/S0022143000209507/type/journal_article](https://www.cambridge.org/core/product/identifier/S0022143000209507/type/journal_article) doi:
479 <https://doi.org/10.3189/172756505781829188>
- 480 Kabore, B. W., Peters, B., Michael, M., & Nicot, F. (2021, 5). A discrete element
481 framework for modeling the mechanical behaviour of snow—Part I: Mechan-
482 ical behaviour and numerical model. *Granular Matter*, 23(2), 42. Retrieved
483 from <https://link.springer.com/10.1007/s10035-020-01083-1> doi:
484 <https://doi.org/10.1007/s10035-020-01083-1>
- 485 Kirchner, H. O., Michot, G., Narita, H., & Suzuki, T. (2001). Snow as a foam of
486 ice: Plasticity, fracture and the brittle-to-ductile transition. *Philosophical Mag-*
487 *azine A*, 81(9), 2161–2181. Retrieved from [http://dx.doi.org/10.1080/](http://dx.doi.org/10.1080/01418610108217141)
488 [01418610108217141](http://dx.doi.org/10.1080/01418610108217141) doi: <https://doi.org/10.1080/01418610108217141>
- 489 Köchle, B., & Schneebeli, M. (2014, 7). Three-dimensional microstructure and nu-
490 merical calculation of elastic properties of alpine snow with a focus on weak
491 layers. *Journal of Glaciology*, 60(222), 705–713. Retrieved from [https://](https://www.cambridge.org/core/product/identifier/S0022143000203067/type/journal_article)
492 [www.cambridge.org/core/product/identifier/S0022143000203067/type/](https://www.cambridge.org/core/product/identifier/S0022143000203067/type/journal_article)
493 [journal_article](https://www.cambridge.org/core/product/identifier/S0022143000203067/type/journal_article) doi: <https://doi.org/10.3189/2014JoG13J220>
- 494 Kojima, K. (1967). Densification of seasonal snow cover. *Physics of Snow and Ice:*

- 495 *proceedings*, 1(2), 929–952.
- 496 Kry, P. R. (1975, 1). The Relationship between the Visco-Elastic and Structural
497 Properties of Fine-Grained Snow. *Journal of Glaciology*, 14(72), 479–500.
498 Retrieved from [https://www.cambridge.org/core/product/identifier/
499 S0022143000021985/type/journal_article](https://www.cambridge.org/core/product/identifier/S0022143000021985/type/journal_article) doi: [https://doi.org/
500 10.3189/S0022143000021985](https://doi.org/10.3189/S0022143000021985)
- 501 Lebensohn, R. A., Montagnat, M., Mansuy, P., Duval, P., Meyssonier, J., & Philip,
502 A. (2009). Modeling viscoplastic behavior and heterogeneous intracrystalline
503 deformation of columnar ice polycrystals. *Acta Materialia*, 57(5), 1405–1415.
504 Retrieved from <http://dx.doi.org/10.1016/j.actamat.2008.10.057> doi:
505 <https://doi.org/10.1016/j.actamat.2008.10.057>
- 506 Lehning, M., Bartelt, P., Brown, B., Fierz, C., & Satyawali, P. K. (2002,
507 11). A physical SNOWPACK model for the Swiss avalanche warning.
508 *Cold Regions Science and Technology*, 35(3), 147–167. Retrieved from
509 <https://linkinghub.elsevier.com/retrieve/pii/S0165232X02000733>
510 doi: [https://doi.org/10.1016/S0165-232X\(02\)00073-3](https://doi.org/10.1016/S0165-232X(02)00073-3)
- 511 Lundin, J. M., Stevens, C. M., Arthern, R., Buizert, C., Orsi, A., LIGTENBERG,
512 S. R., ... WADDINGTON, E. D. (2017, 6). Firn Model Intercomparison
513 Experiment (FirnMICE). *Journal of Glaciology*, 63(239), 401–422. Re-
514 trieved from [https://www.cambridge.org/core/product/identifier/
515 S0022143016001143/type/journal_article](https://www.cambridge.org/core/product/identifier/S0022143016001143/type/journal_article) doi: [https://doi.org/
516 10.1017/jog.2016.114](https://doi.org/10.1017/jog.2016.114)
- 517 Mansuy, P., Philip, A., & Meyssonier, J. (2000). Identification of strain hetero-
518 geneities arising during deformation of ice. *Annals of Glaciology*, 30, 121–126.
- 519 Mellor, M. (1975). A review of basic snow mechanics. *International Association of
520 Hydrological Sciences Publication*, 114(Symposium at Grindelwald 1974 - Snow
521 mechanics), 251–291.
- 522 Mellor, M., & Testa, R. (1969). Effect of Temperature on the Creep of Ice.
523 *Journal of Glaciology*, 8(52), 131–145. doi: [https://doi.org/10.3189/
524 s0022143000020803](https://doi.org/10.3189/s0022143000020803)
- 525 Meyssonier, J., Philip, A., Capolo, L., & Mansuy, P. (2009a). Experimental studies
526 of the viscoplasticity of ice and snow. In D. Kolymbas & G. Viggiani (Eds.),
527 *Mechanics of natural solids* (pp. 203–221). Springer Berlin Heidelberg. doi:
528 https://doi.org/10.1007/978-3-642-03578-4_{_}9
- 529 Meyssonier, J., Philip, A., Capolo, L., & Mansuy, P. (2009b). Experimental stud-
530 ies of the viscoplasticity of ice and snow. In D. Kolymbas & G. Viggiani (Eds.),
531 *Mechanics of natural solids* (pp. 203–221). Berlin, Heidelberg: Springer Berlin
532 Heidelberg. Retrieved from https://doi.org/10.1007/978-3-642-03578-4_9
533 doi: https://doi.org/10.1007/978-3-642-03578-4_{_}9
- 534 Montagnat, M., Bourcier, M., Philip, A., Bons, P. D., Bauer, C. C., Deconinck, P.,
535 & Hereil, P. (2021). Texture characterization of some large hailstones with
536 an automated technique. *Journal of Glaciology*, 67(266), 1190–1204. doi:
537 <https://doi.org/10.1017/jog.2021.66>
- 538 Montagnat, M., Castelnau, O., Bons, P. D., Faria, S. H., Gagliardini, O., Gillet-
539 Chaulet, F., ... Suquet, P. (2014). *Multiscale modeling of ice deformation
540 behavior* (Vol. 61). doi: <https://doi.org/10.1016/j.jsg.2013.05.002>
- 541 Montagnat, M., Chauve, T., Barou, F., Tommasi, A., Beausir, B., & Fressengeas,
542 C. (2015). Analysis of dynamic recrystallization of ice from ebsd orientation
543 mapping. *Frontiers in Earth Science*, 3, 81.
- 544 Morin, S., Horton, S., Techel, F., Bavay, M., Coléou, C., Fierz, C., ... Vionnet,
545 V. (2020, 2). Application of physical snowpack models in support of
546 operational avalanche hazard forecasting: A status report on current im-
547 plementations and prospects for the future. *Cold Regions Science and
548 Technology*, 170(October 2019), 102910. Retrieved from [http://www
549 .sciencedirect.com/science/article/pii/S0165232X19302071](http://www.sciencedirect.com/science/article/pii/S0165232X19302071)<https://>

- linkinghub.elsevier.com/retrieve/pii/S0165232X19302071https://
 550 doi.org/10.1016/j.coldregions.2019.102910 doi: https://doi.org/
 551 10.1016/j.coldregions.2019.102910
 552
- 553 Peinke, L., Hagenmuller, P., Andò, E., Chambon, G., Flin, F., & Roulle, J. (2020,
 554 3). Experimental Study of Cone Penetration in Snow Using X-Ray To-
 555 mography. *Frontiers in Earth Science*, 8, 63. Retrieved from https://
 556 www.frontiersin.org/article/10.3389/feart.2020.00063https://
 557 www.frontiersin.org/article/10.3389/feart.2020.00063/full doi:
 558 https://doi.org/10.3389/feart.2020.00063
- 559 Peters, B., Kabore, B. W., Michael, M., & Nicot, F. (2021). A discrete ele-
 560 ment framework for modeling the mechanical behaviour of snow Part II:
 561 model validation. *Granular Matter*, 23(2). Retrieved from https://
 562 doi.org/10.1007/s10035-020-01084-0 doi: https://doi.org/10.1007/
 563 s10035-020-01084-0
- 564 Petrovic, J. J. (2003). Mechanical properties of ice and snow. *Journal of Materials*
 565 *Science*, 38, 1–6.
- 566 Raj, R., & Ashby, M. (1971). On grain boundary sliding and diffusional creep. *Met-*
 567 *allurgical transactions*, 2, 1113–1127.
- 568 Reuter, B., Proksch, M., Löwe, H., van Herwijnen, A., & Schweizer, J. (2019,
 569 2). Comparing measurements of snow mechanical properties relevant
 570 for slab avalanche release. *Journal of Glaciology*, 65(249), 55–67. Re-
 571 trieved from https://www.cambridge.org/core/product/identifier/
 572 S002214301800093X/type/journal_article doi: https://doi.org/
 573 10.1017/jog.2018.93
- 574 Riche, F., Montagnat, M., & Schneebeli, M. (2013). Evolution of crystal orienta-
 575 tion in snow during temperature gradient metamorphism. *Journal of Glaciol-*
 576 *ogy*, 59(213), 47–55. doi: https://doi.org/10.3189/2013JoG12J116
- 577 Scapozza, C., & Bartelt, P. (2003). Triaxial tests on snow at low strain rate. part ii.
 578 constitutive behaviour. *Journal of Glaciology*, 49(164), 91–101. doi: https://
 579 doi.org/10.3189/172756503781830890
- 580 Schneebeli, M. (2004, 9). Numerical simulation of elastic stress in the microstruc-
 581 ture of snow. *Annals of Glaciology*, 38, 339–342. Retrieved from https://
 582 www.cambridge.org/core/product/identifier/S0260305500256231/type/
 583 journal_article doi: https://doi.org/10.3189/172756404781815284
- 584 Schultz, T., Müller, R., Gross, D., & Humbert, A. (2022). On the contribution
 585 of grain boundary sliding type creep to firn densification - An assessment
 586 using an optimization approach. *The Cryosphere*, 16(1), 143–158. doi:
 587 https://doi.org/10.5194/tc-16-143-2022
- 588 Shapiro, L. H., Johnson, J. B., Sturm, M., & Blaisdell, G. L. (1997). Snow me-
 589 chanics - Review of the state of knowledge and applications. *CRREL Report*,
 590 97(3).
- 591 Simson, A., Löwe, H., & Kowalski, J. (2021). Elements of future snowpack model-
 592 ing – part 2: A modular and extendable eulerian–lagrangian numerical scheme
 593 for coupled transport, phase changes and settling processes. *The Cryosphere*,
 594 15(12), 5423–5445. Retrieved from https://tc.copernicus.org/articles/
 595 15/5423/2021/ doi: https://doi.org/10.5194/tc-15-5423-2021
- 596 Srivastava, P. K., Mahajan, P., Satyawali, P. K., & Kumar, V. (2010, 9). Obser-
 597 vation of temperature gradient metamorphism in snow by X-ray computed
 598 microtomography: measurement of microstructure parameters and simula-
 599 tion of linear elastic properties. *Annals of Glaciology*, 51(54), 73–82. doi:
 600 https://doi.org/10.3189/172756410791386571
- 601 Sundu, K., Ottersberg, R., Jaggi, M., & Löwe, H. (2024). A grain-size driven transi-
 602 tion in the deformation mechanism in slow snow compression. *Acta Materialia*,
 603 262, 119359.
- 604 Suquet, P., Moulinec, H., Castelnau, O., Montagnat, M., Lahellec, N., Grennerat,

- 605 F., ... Brenner, R. (2012). Multi-scale modeling of the mechanical behavior
606 of polycrystalline ice under transient creep. *Procedia IUTAM*, 3, 76–90. doi:
607 <https://doi.org/10.1016/j.piutam.2012.03.006>
- 608 Theile, T., Löwe, H., Theile, T., & Schneebeli, M. (2011). Simulating creep of snow
609 based on microstructure and the anisotropic deformation of ice. *Acta Materi-*
610 *alia*, 59(18), 7104–7113.
- 611 Vionnet, V., Brun, E., Morin, S., Boone, A., Faroux, S., Le Moigne, P., ...
612 Willemet, J.-M. (2012). The detailed snowpack scheme Crocus and its imple-
613 mentation in SURFEX v7 . 2. *Geoscientific Model Development*, 5, 773–791.
614 doi: <https://doi.org/10.5194/gmd-5-773-2012>
- 615 Védérine, L., Hagenmuller, P., Gélébart, L., Montagnat, M., & Bernard, A. (2023,
616 December). *Supplementary data for "Role of ice mechanics on snow vis-*
617 *coplasticity" [Dataset, Codes and Software]*. Zenodo. Retrieved from
618 <https://doi.org/10.5281/zenodo.10340967> doi: [https://doi.org/](https://doi.org/10.5281/zenodo.10340967)
619 [10.5281/zenodo.10340967](https://doi.org/10.5281/zenodo.10340967)
- 620 Wautier, A., Geindreau, C., & Flin, F. (2015). Linking snow microstructure to its
621 macroscopic elastic stiffness tensor: A numerical homogenization method and
622 its application to 3-D images from X-ray tomography. *Geophysical Research*
623 *Letters*, 42(19), 8031–8041. doi: <https://doi.org/10.1002/2015GL065227>
- 624 Wautier, A., Geindreau, C., & Flin, F. (2017, 6). Numerical homogenization
625 of the viscoplastic behavior of snow based on X-ray tomography images.
626 *The Cryosphere*, 11(3), 1465–1485. doi: [https://doi.org/10.5194/](https://doi.org/10.5194/tc-11-1465-2017)
627 [tc-11-1465-2017](https://doi.org/10.5194/tc-11-1465-2017)
- 628 Yosida, Z., Oura, H., Kuroiwa, D., Tosio, H., Kenji, K., & Kinoshita, S. (1958). Phys-
629 ical studies on deposited snow. IV Mechanical properties (3). *Contributions*
630 *from the Institute of Low Temperature Science (Sapporo)*.